



# Sensitivity Identification of Low-Frequency Cantilever Fibre Bragg Grating Accelerometer

Nor Syukriah Khalid<sup>1,2</sup>, Mohd Firdaus Hassan<sup>1\*</sup>

<sup>1</sup>Department of Mechanical Engineering, College of Engineering,  
Universiti Malaysia Pahang, Kuantan, 26300 Pahang, MALAYSIA

<sup>2</sup>DRB-HICOM  
University of Automotive Malaysia, Pekan, 26607 Pahang, MALAYSIA

DOI: <https://doi.org/10.30880/ijie.2021.13.07.027>

Received 1 September 2021; Accepted 15 September 2021; Available online 30 September 2021

**Abstract:** Vibration response of low-frequency cantilever fibre Bragg grating (FBG) accelerometer produced by Euler–Bernoulli model (namely FBG-MM model) is found to be frequency-dependent, unsimilar to SDOF model. Therefore, the sensitivity of the cantilever FBG accelerometer could not be identified using polynomial or basic fitting methods. This paper presents the use of cascade-forward backpropagation neural network (CFB) to predict the sensitivity of the cantilever FBG accelerometer in a "black box", which refers to the behaviour of the deep neural network. The inputs of the network are maximum base accelerations and forcing frequencies, which was set between 20 and 90 Hz (below than the first fundamental frequency of the proposed FBG accelerometer), while the output is the wavelength shift. The validation results show that the wavelength shift predicted by the trained CFB demonstrates good agreement with the FBG-MM, with the input parameter within the range of that used in training process. In addition, results also show that the trained CFB would be invalid if the input parameter is out of the range of that used in training process. In real acceleration measurement, since the forcing frequency is unknown beforehand, the trained CFB must be re-trained by considering the maximum base accelerations are embedded with forcing frequencies.

**Keywords:** Fibre Bragg grating accelerometer, sensitivity, cantilever Euler-Bernoulli beam model, cascade-forward backpropagation neural network

## 1. Introduction

The superior advantages of fibre Bragg grating (FBG) as a transducer have led to the increased interest among the researchers and industrial players. FBG has the capability to operate in unsafe environmental conditions, is able to provide multiple sensing points in a single cable and has remote sensing and invulnerability to electromagnetic fields. These advantages allow FBG to serve in many measurement fields, such as vibration monitoring in gas exploration, military vehicles, footbridge [1-4]; pressure measurement in pipe line leakage detection [5]; temperature monitoring system in lubricating oil, aircraft engine control system [6] etc. In acceleration measurement, the main concern of FBG is its sensitivity, which is related to the reliability of the accelerometer. The sensitivity value of FBG accelerometer has been previously addressed by Teven et al. [7], with less than 1  $\mu\text{g}$  produced by a simple harmonic oscillator. The Fabry-Perot accelerometer which was introduced by Kersey et al. [8] managed to produce high sensitivity and good linearity but not sensitivity value is reported. Gerges et al. [9] then adapted and integrated the principle of Fabry–Perot with diaphragm-type FBG accelerometer for the improvement of the sensitivity. The successful work by Gerges et al. was then continually studied by Weng et al. [10] but with the combination of U-shape rigid cantilever beam, which produced 100 pm/g. This new mechanism was introduced to enhance the vibration effect. To minimise the cross-coupling of non-directional accelerations, Muller et al. [11] had introduced the double diaphragms FBG accelerometer, in which the sensitivity

reported was 1 pm/g. The concept of double diaphragms with different design was also presented by Liu et al. [12], reporting a sensitivity of 45.9 pm/g.

Meanwhile, there are two process methods for determining the sensitivity of the FBG accelerometer: (i) Prediction of the sensitivity using numerical data computed from the mathematical model of the FBG accelerometer; and (ii) Sensitivity identification using empirical data obtained from real acceleration measurement. Li et al. [13] has proposed an ultra-small FBG accelerometer and its sensitivity from the numerical and empirical data was found to be 244 pm/g and 633 pm/g, respectively. Both the numerical and empirical data generated 5 Hz forcing frequency and a steady increment of base acceleration. In contrast to Li et al. [13], Liu et al. [14] computed the sensitivity of symmetrical bended spring plates FBG accelerometer using: (i) numerical data at a single maximum base acceleration of 1 m/s<sup>2</sup> at two forcing frequencies of 5 and 10 Hz; and (ii) empirical data at maximum base acceleration within the range of 1–6 m/s<sup>2</sup> and at forcing frequencies of 5, 10, 15, and 20 Hz (see Fig. 1). From the numerical data, the sensitivity obtained was 1067 pm/g, which is similar to that found using empirical data. Nevertheless, the sensitivity of the FBG accelerometer slightly increased with increasing forcing frequencies (1067 pm/g at 5 Hz, 1084 pm/g at 10 Hz, 1126 pm/g at 15 Hz, and 1166 pm/g at 20 Hz).

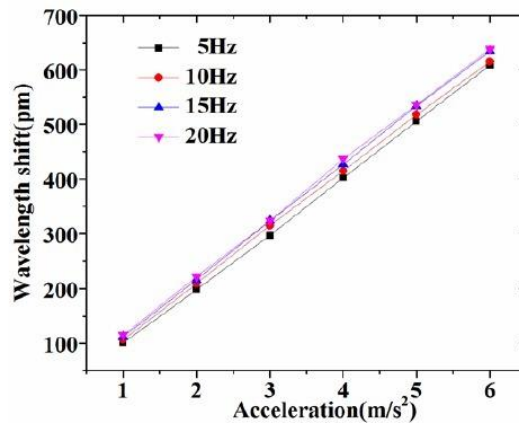


Fig. 1 - Response of the FBG accelerometer under different base accelerations and frequencies [14]

Based on the findings in [14], it can be concluded that the wavelength shift of FBG accelerometer is frequency-dependent. As proposed in a previous work [15], the cantilever FBG accelerometer was modelled using a more accurate approach, namely, FBG-MM. Using the FBG-MM, it is noticed that the predicted amount wavelength shift was found to be frequency-dependent, but the sensitivity is not yet discussed. Hence, this paper proposes cascade-forward backpropagation neural network to identify the sensitivity of cantilever FBG accelerometer to cater for frequency-dependent issues.

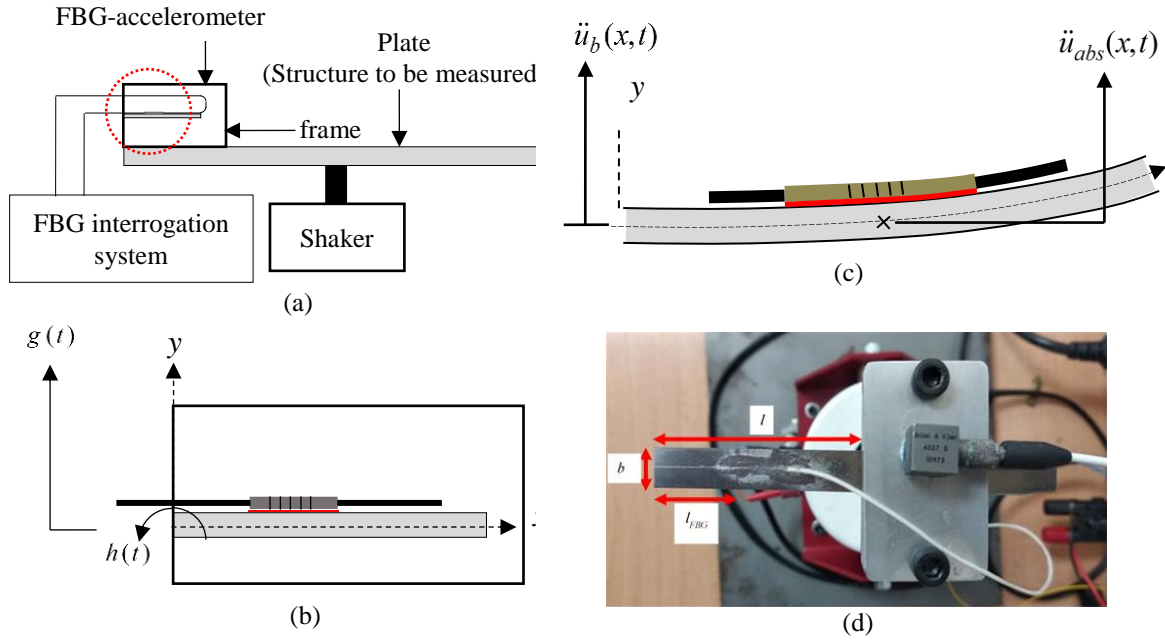
## 2. Basis for Non-Parametric Identification

Fig. 2 shows the measurement configuration of cantilever FBG accelerometer and its absolute motion due to the base motion. The base excitation given to the FBG accelerometer resulted in the computation of the strain based on the relativity between the absolute motion and the base motion. Detailed derivation for the relative motion of cantilever FBG accelerometer is reported in previous publication [15].

The basis for the identification can be constructed by studying the mathematical model of the cantilever FBG accelerometer resulted from the employing of Euler–Bernoulli theorem and modal model approach, namely, FBG-MM [15]. The steady-state response of the cantilevered FBG accelerometer under base excitation is given as:

$$u_{rel}(x, t) = 2U_0 e^{i\omega t} \sum_{r=1}^{\infty} \left( \left[ \cos \square \frac{\lambda_r}{L} x - \cos \frac{\lambda_r}{L} x - \sigma_r \left( \sin \square \frac{\lambda_r}{L} x - \sin \frac{\lambda_r}{L} x \right) \right] \frac{\sigma_r \omega^2}{\lambda_r \omega_r^2 - \omega^2} \right) \quad (1)$$

where,  $U_0 e^{i\omega t}$ ,  $\sigma_r$ ,  $\omega_r$ ,  $\omega$ ,  $\lambda_r$  are harmonic base displacement, a constant for mode ‘r’, natural frequency of mode ‘r’, forcing frequency, and dimensionless frequency numbers, respectively. Eq. 1 is used for computing the curvature of the beam (Eq. 3), which reflects to the amount of strain and wavelength shift of the FBG sensor.



**Fig. 2 - (a) Measurement configuration using cantilever FBG accelerometer; (b) close-up of cantilevered FBG accelerometer (red dotted circle) under translational and rotational base motions; c) absolute motion of FBG due to base motion accelerated by shaker; (d) actual cantilever FBG accelerometer**

The strain of the FBG sensor is given as:

$$\varepsilon_{FBG}(x, t) = -(\square + \square_f) \frac{\partial^2 u_{rel}(x, t)}{\partial x^2} \quad (2)$$

where,

$$\frac{\partial^2 u_{rel}(x, t)}{\partial x^2} = 2U_0 e^{i\omega t} \sum_{r=1}^{\infty} \left(\frac{\lambda_r}{L}\right)^2 \left( \left[ \cos \square \frac{\lambda_r}{L} x + \cos \frac{\lambda_r}{L} x - \sigma_r \left( \sin \square \frac{\lambda_r}{L} x + \sin \frac{\lambda_r}{L} x \right) \right] \frac{\sigma_r \omega^2}{\lambda_r \omega_r^2 - \omega^2} \right) \quad (3)$$

It is known that the wavelength shift of the FBG is directly proportional to the strain of the FBG, as given in Eq. (4) [16, 17].

$$\Delta\lambda \approx 1.2 \times \varepsilon_{FBG}(x, t) \quad (4)$$

where, 1.2 represents the strain sensitivity of FBG with peak wavelengths in the C band regime (1.2 pm/με in general). As compared to SDOF model proposed by [18], the strain of the FBG is given as:

$$\varepsilon_{FBG} = \frac{6(L-x)m}{bd^2E} \ddot{u}_b(x, t) \quad (5)$$

The sensitivity of the FBG sensor is given as:

$$S = \frac{\Delta\lambda}{\ddot{u}_b(x, t)} \quad (6)$$

Replacing both FBG-MM (Eq. 2)) and SDOF model (Eq. (5)) into Eq. (6) resulted in the sensitivity of the FBG accelerometer, as per Eqs. (7) and (8).

$$S_{FBG-MM} = \frac{1.2 \times \varepsilon_{FBG}}{\ddot{u}_b(x, t)} \quad (7)$$

$$S_{SDOF} = \frac{7.2(L-x)m}{bd^2E} \quad (8)$$

It is clearly observed that the sensitivity computed by FBG-MM model (Eq. 7) does depend on the position of FBG sensor (x), time (t), and the forcing frequency (ω). In contrast, the SDOF model (Eq. 8) only depends on the position of FBG

sensor ( $x$ ) and is no longer dependent on time ( $t$ ) and forcing frequency ( $\omega$ ). The plots of wavelength shift against base acceleration for both FBG-MM model and SDOF model are shown in Fig. 3 and Fig. 4, respectively. For SDOF model (Fig. 4), the wavelength shift linearly increases as the base acceleration increases without being affected by the varying forcing frequencies. Nevertheless, the wavelength shift computed by FBG-MM (Fig. 3) was considerably affected by the forcing frequencies, leading to difficulties in identifying its sensitivity.

The sensitivity of the FBG accelerometer SDOF model can be easily determined using simple polynomial function but for FBG-MM, polynomial function may lead to inconsistency in predicted wavelength shift. Therefore, one of the best candidates to determine its sensitivity is using artificial intelligence, such as genetic algorithm (GA) and fuzzy logic, among others. In this paper, the authors prefer to propose neural network identification because it has been successfully used by the co-author of this work in identifying the foil-air bearing forces [19].

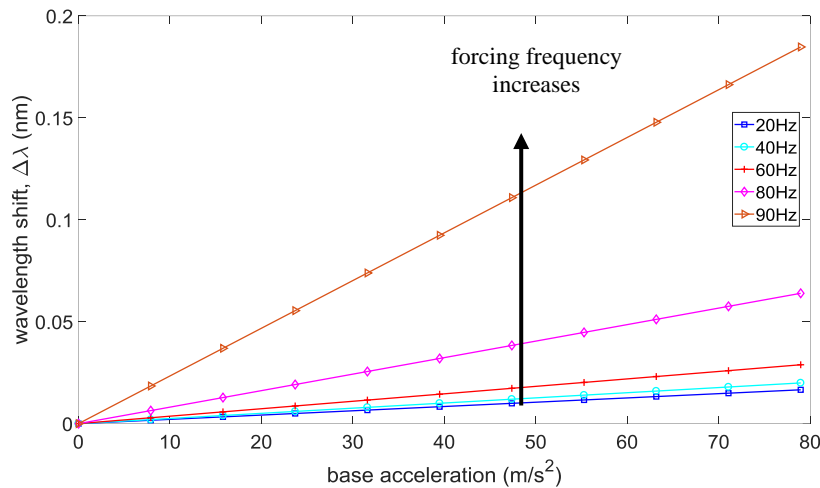


Fig. 3 - The wavelength shift plot against base excitation for FBG-MM

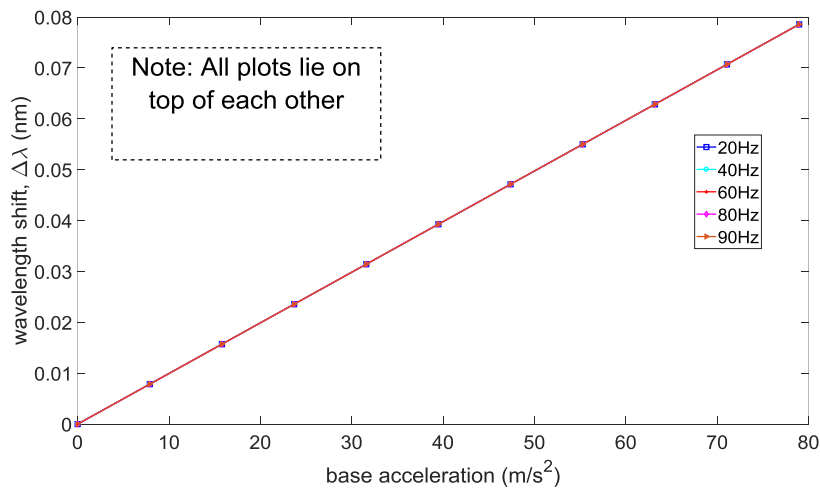


Fig 4. - The wavelength shift plot against base excitation for SDOF model

### 3. Neural Network Identification

Cascade-forward backpropagation neural network (CFB) is proposed to be a non-parametric model for this study, in which the inputs from every previous layer are fed to following layers [20]. The schematic diagram of the network for  $\Delta\lambda$ , and the scheme used to train it, is illustrated in Fig. 5. The CFB's external inputs will be the base acceleration  $\ddot{u}_b(x, t)$  and forcing frequency  $\omega$ . The output estimate of the network for  $\Delta\lambda$  is denoted by  $\Delta\tilde{\lambda}$ . The parameters of the CFB are optimised so that the difference (error),  $\delta$ , between the true (FBG-MM) output,  $\Delta\lambda$ , and the network output,  $\Delta\tilde{\lambda}$ , can be minimised to a value below the specific convergence limit/tolerance.

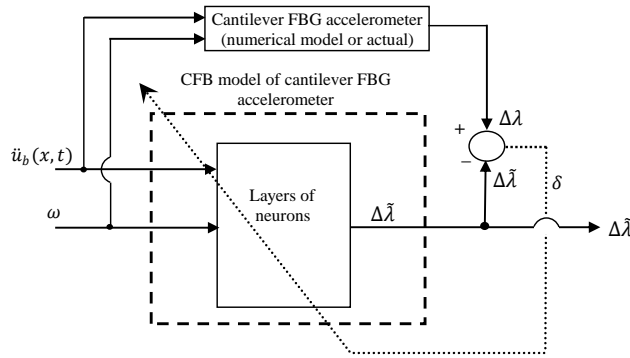


Fig. 5 - CFB model of the wavelength shift  $\Delta\lambda$  and its identification procedure

### 3.1 Training Data Generation

From the aforementioned theory of FBG-MM and Fig. 2 (a), the identification of CFB requires training data sets comprising the true output for the given inputs. These data sets can be generated in two ways, depending on whether the identified cantilever FBG accelerometer is numerical or an actual transducer.

- Cantilever FBG accelerometer is represented by numerical model (FBG-MM) – prescribing  $\ddot{u}_b(x, t)$  and  $\omega$ , and determining the resulting wavelength shift,  $\Delta\lambda$ .
- Cantilever FBG accelerometer is excited by shaker by applying base excitation through voltage input to shaker at known excitation frequencies,  $f_e$ , and determining the resulting base acceleration,  $\ddot{u}_b(x, t)$ , and wavelength shift,  $\Delta\lambda$ .

The input-output data computed by Eq. 1 (after dual-differentiation to obtain  $\ddot{u}_b(x, t)$ ) and Eq. (4) are tabulated in Table 1. The position of FBG sensor,  $x$ , is 30 mm from the fixed end of the cantilever beam.

Table 1 - Input and output data for CFB

Input data 1, $\omega$ ( $2\pi f$ ), where $f$ (Hz)	Input data 2, $\ddot{u}_b(x, t)$ ( $m/s^2$ ) **	Output data, $\Delta\lambda$ (nm)
$2\pi$ ( $f = 1$ Hz) $[\omega_{1 \times 202}] = [2\pi, 2\pi \dots 2\pi]$	$\ddot{u}_b(0.03, t)_{1 \times 202} = [-78.96, -78.17, \dots 0, 0.7896, 1.5792, \dots 78.96]$	$\Delta\lambda = [0, 1.5679e^{-4}, \dots 0.0157]$
$4\pi$ ( $f = 2$ Hz) $[\omega_{1 \times 202}] = [4\pi, 4\pi \dots 4\pi]$	$\ddot{u}_b(0.03, t)_{1 \times 202} = [-78.96, -78.17, \dots 0, 0.7896, 1.5792, \dots 78.96]$	$\Delta\lambda = [0, 1.5685e^{-4}, \dots 0.0157]$
⋮	⋮	⋮
$178\pi$ ( $f = 89$ Hz) $[\omega_{1 \times 202}] = [178\pi, 178\pi \dots 178\pi]$	$\ddot{u}_b(0.03, t)_{1 \times 202} = [-78.96, -78.17, \dots 0, 0.7896, 1.5792, \dots 78.96]$	$\Delta\lambda = [0, 0.0016, \dots 0.1551]$
$180\pi$ ( $f = 90$ Hz) $[\omega_{1 \times 202}] = [180\pi, 180\pi \dots 180\pi]$	$\ddot{u}_b(0.03, t)_{1 \times 202} = [-78.96, -78.17, \dots 0, 0.7896, 1.5792, \dots 78.96]$	$\Delta\lambda = [0, 0.0018, \dots 0.1848]$

\*\* $\ddot{u}_b(0.03, t)$  vary between  $-78.96$  to  $78.96$   $m/s^2$

Input-output data in Table 1 will be generated to the cantilever FBG accelerometer with parameters of cantilever beam and FBG sensor as in Table 2 (used in previous authors’ work[15]). The total input-output data will be  $[2 \times 18180]$  and  $[1 \times 18180]$ , respectively. Noted that the excitation profile is sinusoidal. For validation purpose, the trained CFB will be tested on time-series data over the wide range of forcing frequency and maximum base acceleration as well as at various location of FBG sensor ( $x$ ).

**Table 2 - Properties of cantilever beam and FBG sensor**

Parameter	Value
length, $l$	50 mm
width, $b$	10 mm
thickness, $d$	0.3 mm
location of centre of FBG measured from fixed end, $l_{FBG}$	30 mm
density, $\rho$	8000 kg/m <sup>3</sup>
Young's Modulus, $E$	193 GPa
Poisson ratio, $\nu$	0.29
wavelength of FBG sensor	1544 nm

### 3.2 CFB Architecture and Training

With reference to Fig. 6, the best architecture for CFB after several try-and-error attempts was two hidden layers with 10 and 5 neurons, respectively. Both hidden and output layers used hyperbolic tangent sigmoid transfer function and the Levenberg–Marquardt optimisation method was chosen to optimise the weights and biases of the network. The input-output data set is divided into 70% for training, 15% for validation and 15% for testing. Meanwhile,  $\mathbf{q}_k$  is defined as  $3 \times 18180$  matrix comprising the input to layer no. 1.

$$\mathbf{q}_k = [\ddot{u}_{b_1} \ddot{u}_{b_2} \dots \ddot{u}_{b_{9090}}; \omega_1 \omega_2 \dots \omega_{9090}; \Delta\tilde{\lambda}_1, \Delta\tilde{\lambda}_2 \dots \Delta\tilde{\lambda}_{9090}] \tag{9}$$

The output of the  $l^{st}$  layer as:

$$\mathbf{a}_k^{(1)} = \mathbf{h}^{(1)}(\mathbf{W}^{(1)}\mathbf{a}_k^{(1)} + \mathbf{b}^{(1)}) \tag{10}$$

While the output of the subsequent layer  $m^{th}$  layer are:

$$\mathbf{a}_k^{(m)} = \mathbf{h}^{(m)}(\mathbf{W}^{(m)}\mathbf{a}_k^{(m-1)} + \mathbf{W}^{(m)}\mathbf{a}_k^{(m-2)} + \mathbf{W}^{(m)}\mathbf{a}_k^{(m-3)} \dots \mathbf{W}^{(m)}\mathbf{q}_k + \mathbf{b}^{(m)}), \quad m = 1, 2, \dots, M \tag{11}$$

where,  $\mathbf{W}^{(m)}$  and  $\mathbf{b}^{(m)}$  are the matrix of weights and vector of biases of the  $m^{th}$  layer, respectively; and  $\mathbf{h}^{(m)}(\ )$  is a vector operator comprising the transfer functions of the neurons of the  $m^{th}$  layer.

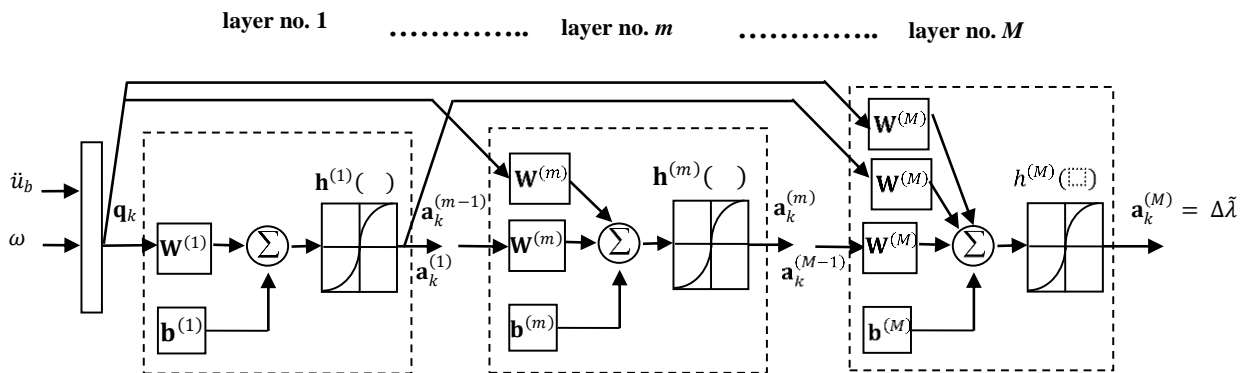


**Fig. 6 - CFB architecture**

### 4. Results and Discussion

In addition to the 15% of input-output data set in CFB training process that was assigned for testing, a new set of input-output data was generated from FBG-MM to be used in testing/validation process to investigate the efficiency of the sensitivity of the trained CFB. Three input-output data set are as follows:

- Set 1 – time-series of input-output (base acceleration-wavelength shift) data with the forcing frequencies are  $1 \text{ Hz} \leq f \leq 90 \text{ Hz}$  and the maximum base acceleration does not exceed  $\pm 78.98 \text{ m/s}^2$  – within the range of the forcing frequencies and the maximum base acceleration used in training process;

- Set 2 – time-series of input-output (base acceleration-wavelength shift) data with the forcing frequencies are  $1 \text{ Hz} \leq f \leq 90 \text{ Hz}$  but the maximum base acceleration exceeding the maximum base acceleration used in training process; and
- Set 3 – time-series of input-output (base acceleration-wavelength shift) data with both forcing frequencies and maximum base acceleration are randomly set and the position of FBG sensor on the cantilever beam was changed from 0.03 m to 0.04 m.

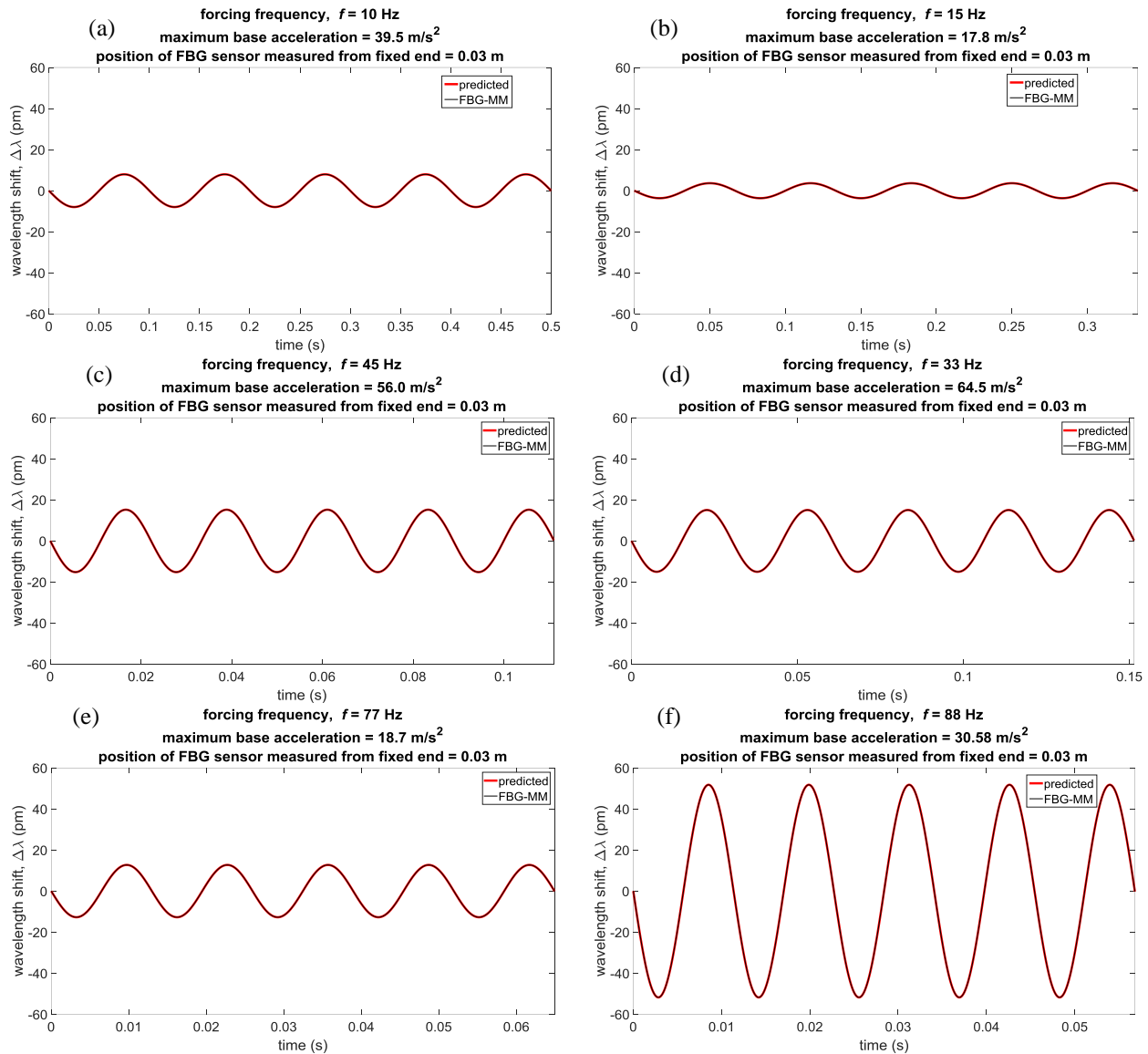


**Fig. 7 - Predicted versus FBG-MM wavelength shift where the forcing frequencies, maximum base acceleration, and position of FBG sensor within the range of that used in training process**

As seen in Fig. 7, it is apparent that the trained CFB could predict the wavelength shift is perfectly well for the input-output data of Set 1, since the forcing frequencies and maximum base acceleration within the range of that used in training process.

In Fig. 8, the input of Set 2 provided the maximum base acceleration exceeding the range as used in training process, thus the trained CFB could not predict the wavelength shift very good. This can be clearly seen in Fig. 8(b), (c), (e), and (f) when the maximum base excitation was set to be 266.5, 215.0, 234.1, and 223.5 m/s<sup>2</sup>. It is also observed that the trained CFB unable to predict the wavelength shift, which was excited by high base excitation, as shown by the green circle in the same figures. Nevertheless, in Fig. (a) and (d), with the maximum base acceleration (158.0 and 114.4 m/s<sup>2</sup>) reasonably close to that used in training process ( $\pm 78.98 \text{ m/s}^2$ ), the prediction is still acceptable with over prediction when the forcing frequencies and base acceleration kept increasing.

Fig. 9 presents the predicted wavelength shift with the position of the FBG on the beam was changed from 0.03 m as used in training process to 0.04 m. It is noted that by changing the position of FBG to other point, e.g., at 0.04 m from

fixed end of the beam, the trained CFB able to predict the pattern of the wavelength shift only and not its magnitude (see Fig. 9 (a)). Its prediction getting worse when the maximum base acceleration increasing even though its forcing frequency remains small, as used in Fig. 9 (a), as shown in Fig. 9 (b). Combination of medium-to-high value of forcing frequency and maximum base acceleration will certainly lead to unacceptable prediction, as seen from Fig. 9 (c) to (f).

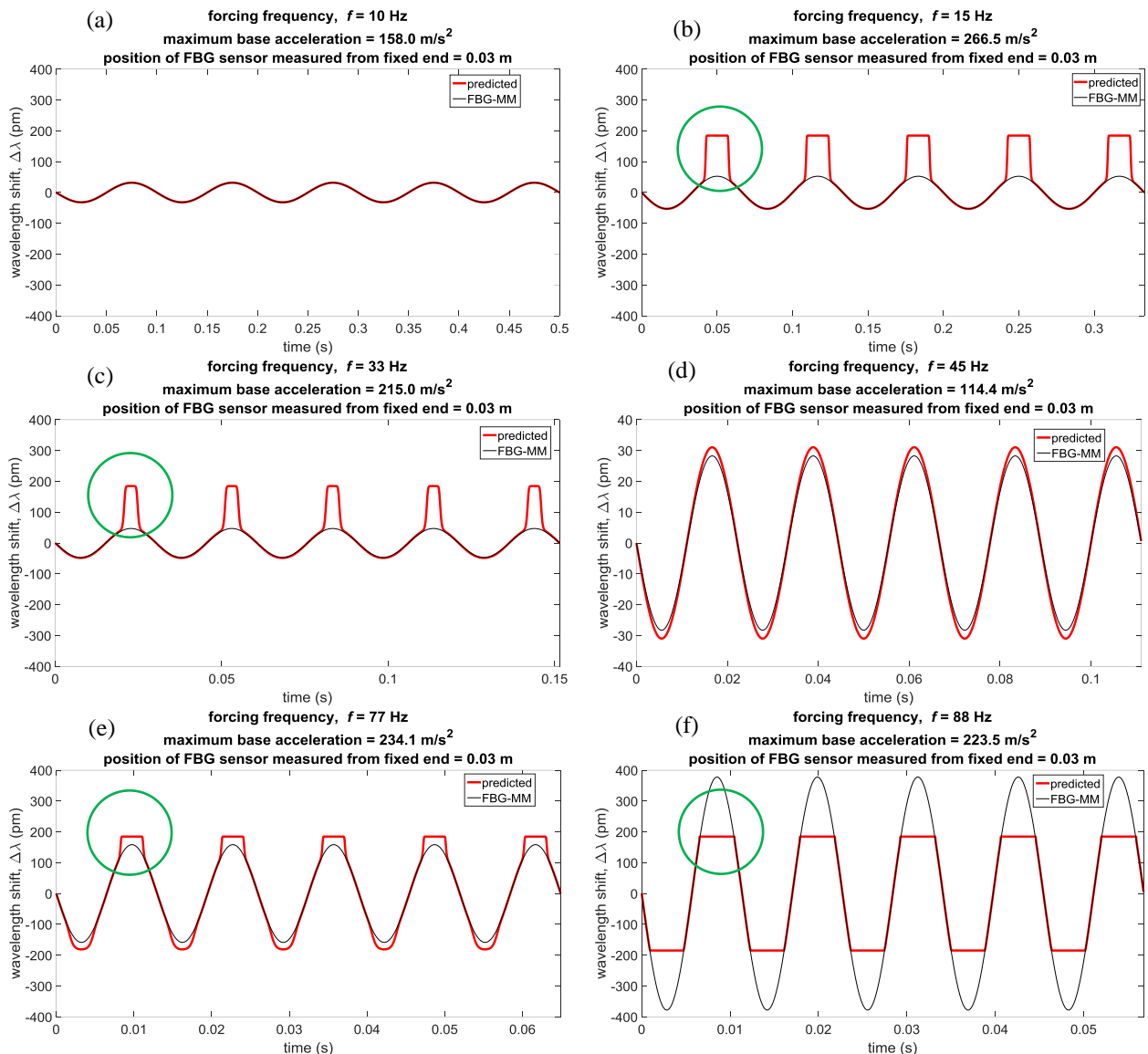


**Fig. 8 - Predicted versus FBG-MM wavelength shift, where the forcing frequencies and position of FBG sensor within the range of that used in training process but with high maximum base acceleration**

### 5. Conclusion

The research shows that the sensitivity of the cantilever FBG accelerometer is able to be identified by neural network because the wavelength shift is frequency-dependent, as opposed to SDOF model. The identified CFB is only valid for the input parameter within the range of that used in the training process. Hence, the robustness of the CFB can be improved if the range of forcing frequency, the maximum base acceleration the variation position of FBG sensor is identified prior to train the CFB. However, in this study, since the fundamental frequency of the proposed cantilever FBG accelerometer is 95.2 Hz, extending the range of forcing frequency is unbeneficial because the effective range of forcing frequency for an accelerometer should be less than its fundamental frequency (range of forcing frequency for CFB was  $1 \text{ Hz} \leq f \leq 90 \text{ Hz}$ ). In actual acceleration measurement, frequency is not known beforehand, thus, using the trained CFB will not work unless it is re-trained without prescribing the forcing frequency. To overcome this issue, the base acceleration can be generated using chirps signal with increasing amplitude, forcing frequency and position of FBG sensor. The use of chirp signal has been successfully applied in the foil-air bearing rotor system by the co-author of this work [19].

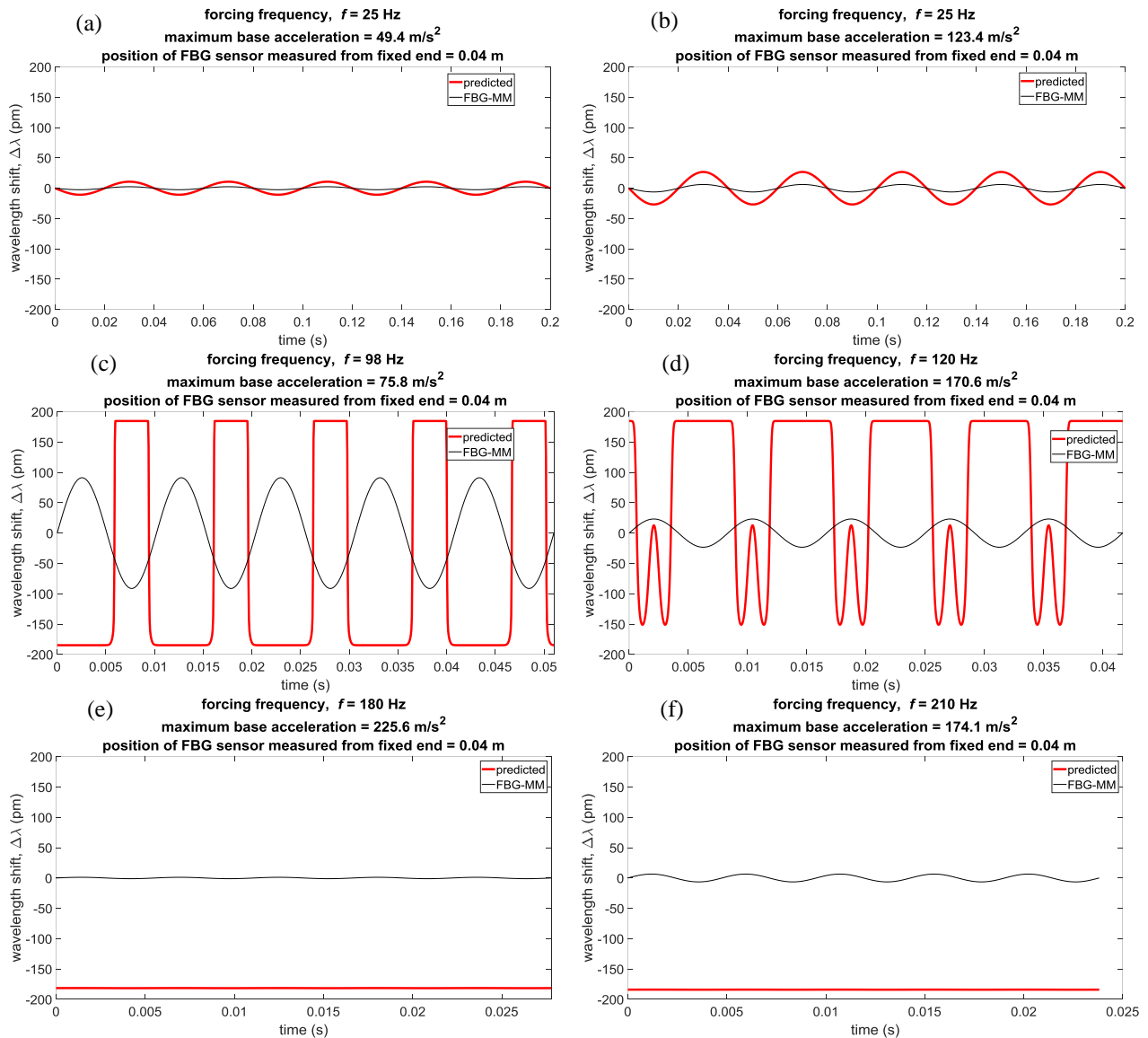


**Fig. 9 - Predicted versus FBG-MM wavelength shift at random forcing frequencies maximum base acceleration but the position of the FBG is changed to 0.04 measured from fixed end**

### Acknowledgement

The authors acknowledge the Ministry of Education Malaysia for their financial support provided under Fundamental Research Grant Scheme (FRGS) No. FRGS/1/2018/TK03/UMP/02/29 (RDU190191). The authors also acknowledge Universiti Malaysia Pahang for their facilities support. Data related to the research presented in this paper shall be made available through the University Malaysia Pahang's Institutional Repository.

### References

- [1] Gagliardi, G., et al., *Design and test of a laser-based optical-fiber Bragg-grating accelerometer for seismic applications*. Measurement Science and Technology, 2008. **19**(8): p. 085306
- [2] Zhang, Y., et al. *Fiber Bragg grating sensors for seismic wave detection*. in *Bruges, Belgium-Deadline Past*. 2005. International Society for Optics and Photonics
- [3] da Costa Antunes, P.F., et al., *Optical fiber accelerometer system for structural dynamic monitoring*. IEEE Sensors Journal, 2009. **9**(11): p. 1347-1354
- [4] Zhang, Y., et al., *Fiber-Bragg-grating-based seismic geophone for oil/gas prospecting*. Optical Engineering, 2006. **45**(8): p. 084404-084404-4
- [5] Huang, J., et al., *A fiber Bragg grating pressure sensor and its application to pipeline leakage detection*. Advances in Mechanical Engineering, 2013. **5**: p. 590451

- [6] Gebru, H.A. and B. Padhy. *Fiber Bragg Grating Temperature Sensor for Defence and Industrial Applications*. in *AIP Conference Proceedings*. 2011. AIP
- [7] Tveten, A., et al., *Fibre optic accelerometer*. Electronics Letters, 1980. **16**(22): p. 854-856
- [8] Kersey, A., D. Jackson, and M. Corke, *A simple fibre Fabry-Perot sensor*. Optics Communications, 1983. **45**(2): p. 71-74
- [9] Gerges, A., et al., *High-sensitivity fiber-optic accelerometer*. Optics letters, 1989. **14**(4): p. 251-253
- [10] Weng, Y., et al., *A robust and compact fiber Bragg grating vibration sensor for seismic measurement*. IEEE Sensors J., 2011. **12**(4): p. 800-804
- [11] Muller, M.S., T.C. Buck, and A.W. Koch. *Fiber Bragg grating-based acceleration sensor*. in *Optomechatronic Technologies, 2009. ISOT 2009. International Symposium on*. 2009. IEEE
- [12] Liu, Q., et al., *Large frequency range and high sensitivity fiber Bragg grating accelerometer based on double diaphragms*. IEEE Sensors Journal, 2014. **14**(5): p. 1499-1504
- [13] Li, K., et al., *Ultra-Small Fiber Bragg Grating Accelerometer*. Applied Sciences, 2019. **9**(13): p. 2707
- [14] Liu, F., et al., *A low frequency FBG accelerometer with symmetrical bended spring plates*. Sensors, 2017. **17**(1): p. 206
- [15] Khalid, N.S., et al., *A strain-wavelength modelling of low-frequency cantilever fibre Bragg grating accelerometer*. Proceedings of the Institution of Mechanical Engineers, Part C: Journal of Mechanical Engineering Science, 2021: p. 09544062211008929
- [16] Basumallick, N., et al., *Design optimisation of fiber Bragg grating accelerometer for maximum sensitivity*. Sensors and Actuators A: Physical, 2013. **194**: p. 31-39
- [17] Basumallick, N., et al., *Fiber Bragg grating accelerometer with enhanced sensitivity*. Sensors and Actuators A: Physical, 2012. **173**(1): p. 108-115
- [18] Lam, T.T., et al., *Optical fiber three-axis accelerometer based on lasers locked to  $\pi$  phase-shifted Bragg gratings*. Measurement Science and Technology, 2010. **21**(9): p. 094010
- [19] Hassan, M.F.B. and P. Bonello, *A neural network identification technique for a foil-air bearing under variable speed conditions and its application to unbalance response analysis*. Journal of Tribology, 2017. **139**(2)
- [20] Beale, M.H., M.T. Hagan, and H.B. Demuth, *Neural network toolbox*. User's Guide, MathWorks, 2010. **2**: p. 77-81